N. Jb. Geol. Paläont. Abh. 281/3, 227–246
Stuttgart, September 2016

Article

Mineral chemistry and geothermometry of Fe-Ti oxides in the Khanlogh magnetite-apatite ore, northwest of Neyshabour, NE Iran

Parvin Najafzadeh Tehrani, Ali Asghar Calagari, Francisco Velasco Roldan, Vartan Simmonds and Kamal Siahcheshm

With 11 figures and 7 tables

Abstract: The Khanlogh iron deposit is located to the northwest of Neyshabour in NE Iran within the Cenozoic Sabzevar-Quchan magmatic arc. The ores are hosted by a series of subvolcanic bodies of intermediate composition (dioritic porphyries) of Oligocene age. Mineralization in the study area occurs as vein, stockwork, disseminations, and open-space fillings of fault breccias within the host rocks. Microscopic and SEM examinations demonstrate that magnetite, apatite, and diopside are the main constituent minerals of the ores. Magnetite crystals contain exsolved inclusions of ilmenite in trellis and dispersed forms. Mineral chemistry data show that the minor oxide constituents in magnetite are V_2O_3 (0.6%), TiO_2 (1.8%), MnO (0.2%), and MgO (0.6%), and in ilmenite include MgO (3.3%), V_2O_3 (1.9%) and MnO (2.6%). The higher amounts of vanadium in ilmenite relative to the host magnetite is due to substitution of V^{4+} for Ti^{4+} in the crystal structure of ilmenite. Geothermometry on magnetite and associated exsolved ilmenite indicate that the Khanlogh iron ores developed at temperatures of approximately 550°C and $fo_2 \approx 10^{-18}$atm. The ore-forming fluids at Khanlogh had high contents of Fe, Ti, and P, and likely originated from calc-alkaline-tholeiitic magmas.

Key words: Magnetite; ilmenite; geothermometry; geochemistry; Khanlogh; Neyshabour.

Introduction

Magnetite and ilmenite are two important minerals in hydrothermal magmatic iron deposits and many studies on the mode of formation of these two minerals in igneous, metamorphic, and various Fe-Ti deposits have been carried out (Philpotts 1967; Kärkkäinen & Appelqvist 1999; Mücke 2003; Clark & Kontak 2004; Charlier et al. 2007; She et al. 2015; Charlier et al. 2015). One of the practical methods for recognizing the physico-chemical conditions of the formation is the distribution of rare elements in magnetite and ilmenite (Dupuis & Beaudoin 2011; Dare et al. 2014; Nadoll et al. 2014; Charlier et al. 2015). The effective parameters controlling the chemical composition of magnetite during deposition include (1) the compositions of parent magma and associated hydrothermal fluids, (2) temperature, (3) pressure, (4) the cooling rate of fluids, (5) oxygen fugacity (fO_2), (6) sulfur fugacity (fS_2), and (7) silica activity (Whalen & Chappell 1988; Frost & Lindsley 1991; Ghiorso & Sack 1991). In magnetite-ilmenite-apatite deposits, the initial composition of the parent magma, fO_2, and presence of volatiles are the most important controlling parameters (She et al. 2015; Charlier et al. 2015). Considering the variations of temperature and fO_2 in various geologic environments, the Ti contents of Fe-Ti oxides differs in various deposits (Buddington & Lindsley 1964; Lindh 1972; Lindsley & Lindh 1974; Oliver 1978; Ghiorso & Sack 1991; Lattard et al. 2005).

www.schweizerbart.de
DOI: 10.1127/njgpa/2016/0597
0077-7749/2016/0597 $ 5.00

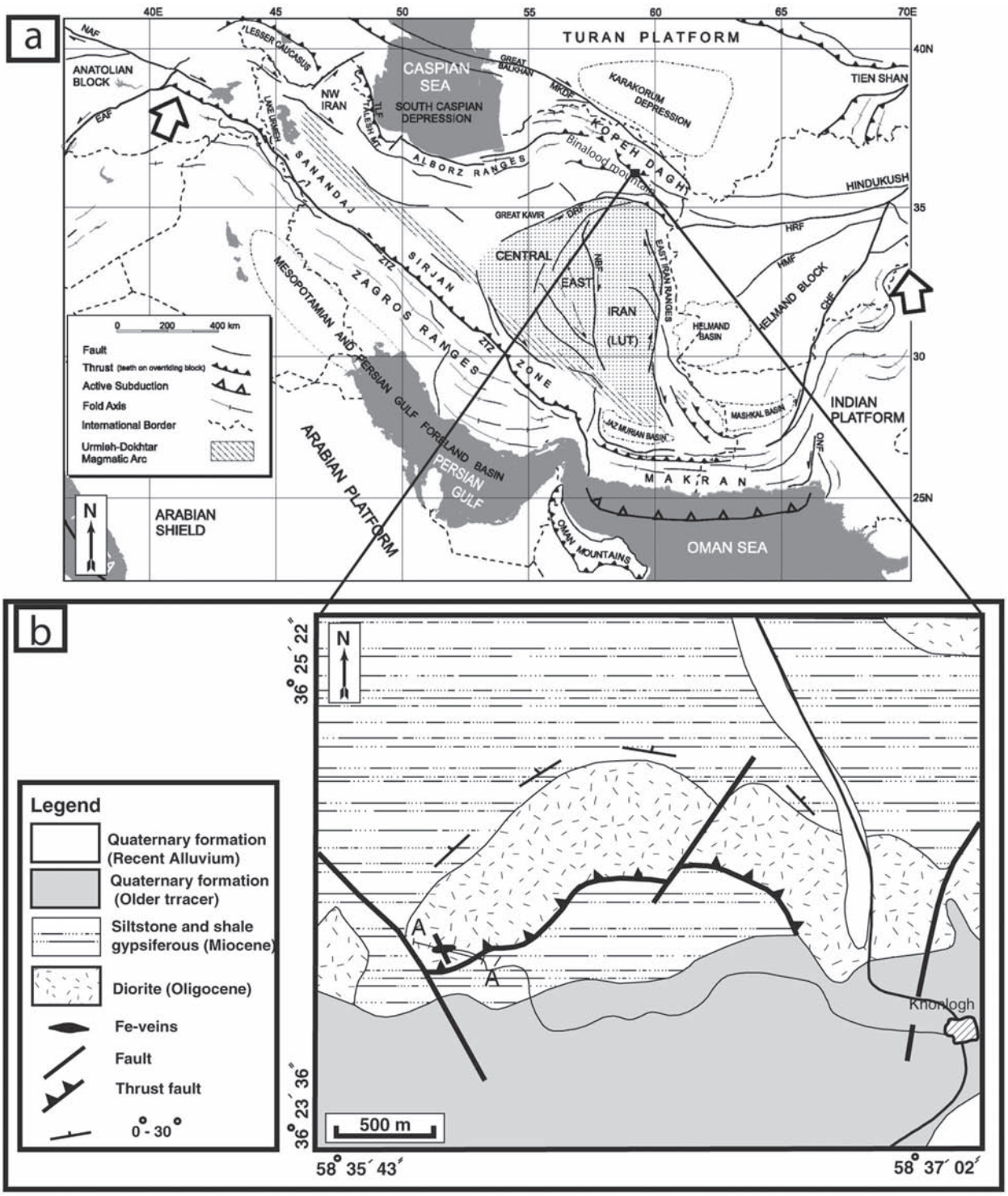

Fig. 1. (a) Location of the study area in the structural zone of Iran (after Ramezani & Tucker 2003). (b) Geologic map of the Khanlogh iron deposit.

The Khanlogh deposit in northeastern Iran formed in Oligocene subvolcanic host overlying the magmatic arc of the Sabsevar-Quchan subduction zone. Iron mineralization occurred as veins and open-space filling in fault breccia zone (Najafzadeh Tehrani et al. 2016). Magnetite is accompanied by considerable amounts of

apatite and diopside. Based upon geochemical studies on the constituent minerals of the ores and the host rocks, Zarei et al. (2016) concluded that the Khanlogh iron ore was of Kiruna-type (IOA, iron-oxide-apatite).

Using electron probe micro-analysis (EPMA), X-ray diffractometry (XRD) and X-ray fluorescence (XRF) analysis, the present study presents the mineralogical and geochemical characteristics of the host rocks as well as stoichiometries of diopside and apatite to thoroughly investigate the relationship between Fe mineralization and the host rocks. Finally, by considering the mineral chemistry of magnetite and ilmenite with respect to vanadium and titanium content, the oxygen fugacity (fO_2) and formation temperature conditions of the iron ores were estimated.

Geology

The Khanlogh iron deposit is located ca. 30 km northwest of Neyshabour and is situated in the northern Binalood structural zone of Nabavi (1976) and Alavi (1992) east of the NW-SE trending Alborz Mountains (Fig. 1a). Lower Paleozoic, Jurassic, Cretaceous, and Cenozoic rock sequences as well as remnants of the Paleo-Tethys oceanic realm were transported in a southwestward direction by several thrust faults of two generations: (1) Cimmerian and (2) Alpine (Alavi 1992). The Binalood mountain range in which the study area is situated is dominated by magmatic rocks of the Sabzevar-Quchan magmatic arc that consists of Eocene calc-alkaline andesites, Oligocene-Pliocene dacites, and Miocene-Pliocene shoshonitic and alkaline basalts (Spies et al. 1983).

The study area itself mainly consists of Oligocene subvolcanic igneous rocks, Miocene sedimentary units and Quaternary alluvia (Fig. 1b). The rocks hosting the Khanlogh iron ores extend up to 4 km in E-W direction and are mainly subvolcanic intrusions with porphyritic textures and fine-grained groundmasses. Miocene units are mainly composed of marls, siltstones and shales containing gypsum lenses. These sedimentary units overlie an Oligocene subvolcanic unit but, due to reverse faulting in the south of the area, are overlain by an Oligocene subvolcanic unit.

Two fault systems (Fig. 1b) caused fracturing and brecciation of the host rocks: a) reverse (Fig. 2a) and b) normal faults (Fig. 2b). As a result, iron-oxide mineralization developed as veins and veinlets of various thicknesses throughout the entire area (Fig. 2c, d). The most important and abundant minerals in the ore are magnetite, diopside, and apatite.

Sampling and laboratory methods

The study of the Khanlogh iron deposit was carried out in the field and in the laboratory. The field works included preparation of the map and sampling of iron ores and host rocks. The laboratory work started with microscopic examinations of 50 thin-polished sections of the ores and host rocks and X-ray diffraction (XRD) analyses for identifying undistinguishable mineral phases in the ores. The chemical composition of the constituent minerals in the ores and host rocks were obtained by electron probe micro-analysis (EPMA). Electron probe micro-analyses were carried out on 4 thin-polished samples and comprise 14 crystals of magnetite (5 crystals), ilmenite (2 crystals), hematite (2 crystals), diopside (4 crystals), and apatite (1 crystal). Electron microprobe (EPMA) analyses were performed in the Mineralogy Laboratory of the Basque Country University using a Camebax/Cameca equipped with 4 vertical spectrometers. Operating conditions for major elements in silicates included an accelerating voltage of 15 kV, an electron beam current of 10 nA and a beam diameter (source region) of 2 µm. Counting times were 30 s on the peak and 10 s on each side of the background. For major elements, international standard from Spi Structure Probe Inc. were used and included: jadeite (Na-10.54%), sanidine (K-10.05%), diopside (Ca-18.39%), spodumene Al-14.50%; Si-30.18%), hematite (Fe-69.94%), olivine (Mg-31.10%), and pure metals (Mn and Ti). For trace elements analysis operating conditions were changed to 50 100 nA and counting times of 90 s. X-ray line interferences between elements were minimized and concentrations were corrected for major element matrix effects using the PAP matrix correction procedure (Pouchou & Pichoir 1984). Detection limits were calculated with an accuracy of 2σ, at 95% confidence level, and are as follows: Ni 700 ppm, Co 700 ppm, Cu 700 ppm, Zn 700 ppm, As 700 ppm.

Representative samples from the iron mineralization and associated volcanic rocks were selected for chemical characterization. All major (as % wt) and trace elements (As, Ba, Co, Cu, Cr, F, Mo, Ni, Nb, Pb, Rb, S, Sr, V, W, Y, Zn, Zr, Cs, Th, Sn; expressed as parts per million (ppm)) were determined by Wavelength Dispersive X-ray Fluorescence (WDXRF) using a PANalytical Axios Advanced PW4400 XRF spectrometer (4 kW Rh anode SST-mAX X-ray tube) at the Servicios Generales de Investigación (SGIker) of the Basque Country University / Euskal Herriko. Fused beads were prepared mixing 0.2 g of finely ground sample with 3.8 g of a lithium borate flux (Spectromelt A12, Merck) and LiBr as non-wetting agent. Lower limit of detection for major elements are in the range of 0.01 wt% and ~5 ppm for trace elements.

For complementary mineralogical studies, four samples from the magnetite-apatite ores were studied by scanning electron microscope (SEM) (LEO-1450VP) at the Iranian Research Center of Mineral Materials.

Fe^{2+} and Fe^{3+} concentrations in the oxide minerals were calculated by, firstly, normalization of the chemical formula to 4 oxygen atoms in the case of magnetite and to 3 oxygen atoms for ilmenite; followed by, calculation of the the ferric iron content of each analysis assuming stoichiometry; i.e. for magnetite with the ideal formula $Fe^{2+}Fe^{3+}O_4$, by assuming stoichiometry and an Fe^{3+}/Fe^{2+} ratio of 2:1 for charge balance.

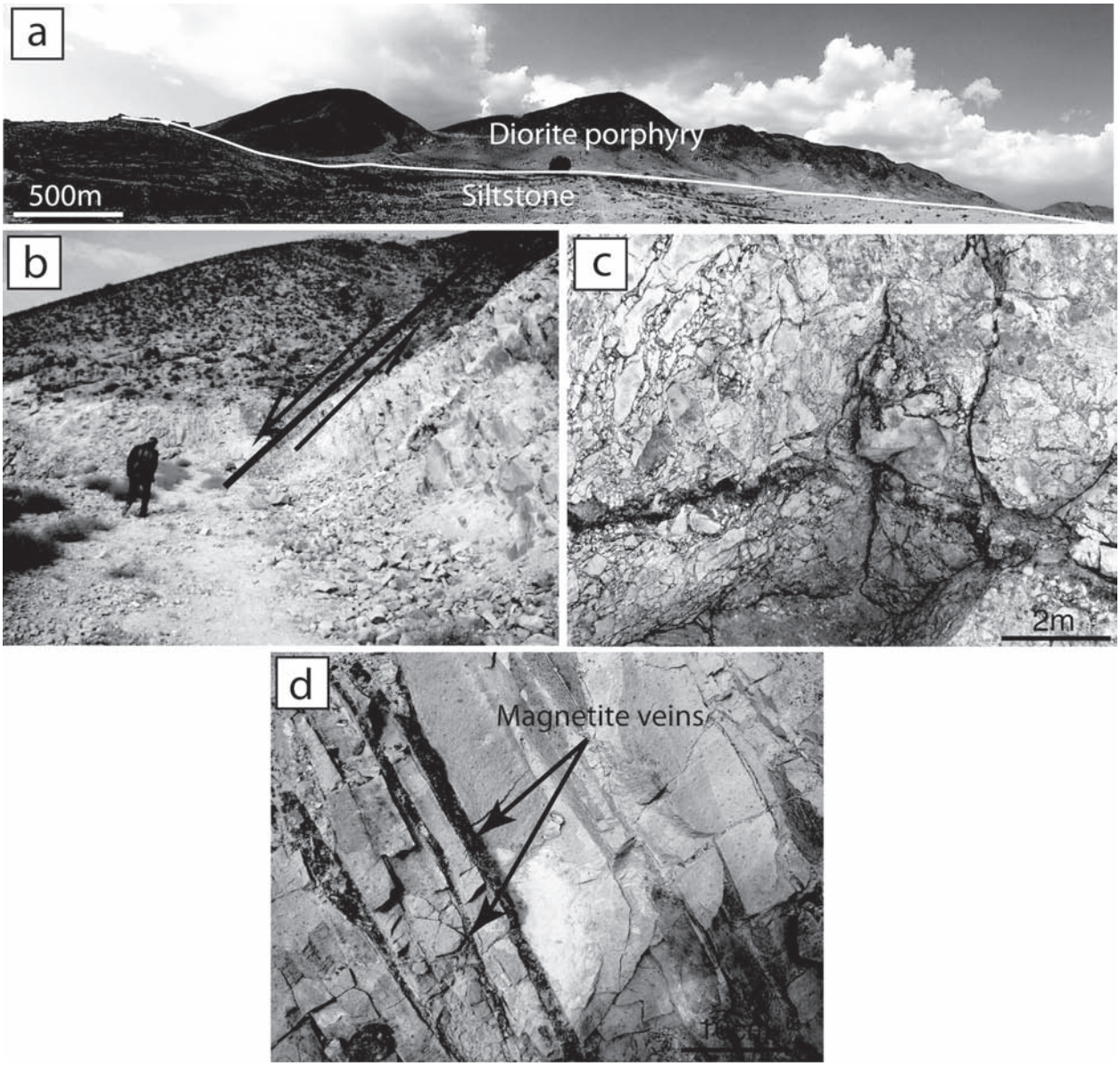

Fig. 2. Field photographs of subvolcanics and iron ores in the Khanlogh area. (a) Oligocene subvolcanic host trusted by a fault over Miocene marl and siltstone (view towards north). (b) Normal fault in diorite porphyry (view towards north). (c) Fault breccias with open spaces filled by iron oxides. (d) magnetite-bearing veins in porphyritic diorite host.

Results and discussion

Petrography of the subvolcanic bodies

Mesoscopically, the subvolcanic host rocks are white to gray with porphyritic textures manifested by feldspar phenocrysts. Microscopically, the samples consist of plagioclase (c. 80%), quartz (<10%) and clinopyroxene (5-10%). Plagioclase occurs as fine- to medium-grained (2-10 mm) subhedral to euhedral phenocryst and as fine-grained aphanitic crystals in the matrix and is partially replaced by sericite. Clinopyroxenes are fine-grained (0.1-1 mm) subhedral to euhedral crystals and are occasionally replaced by calcite. Quartz occurs as fine-grained crystals dispersed in the groundmass.

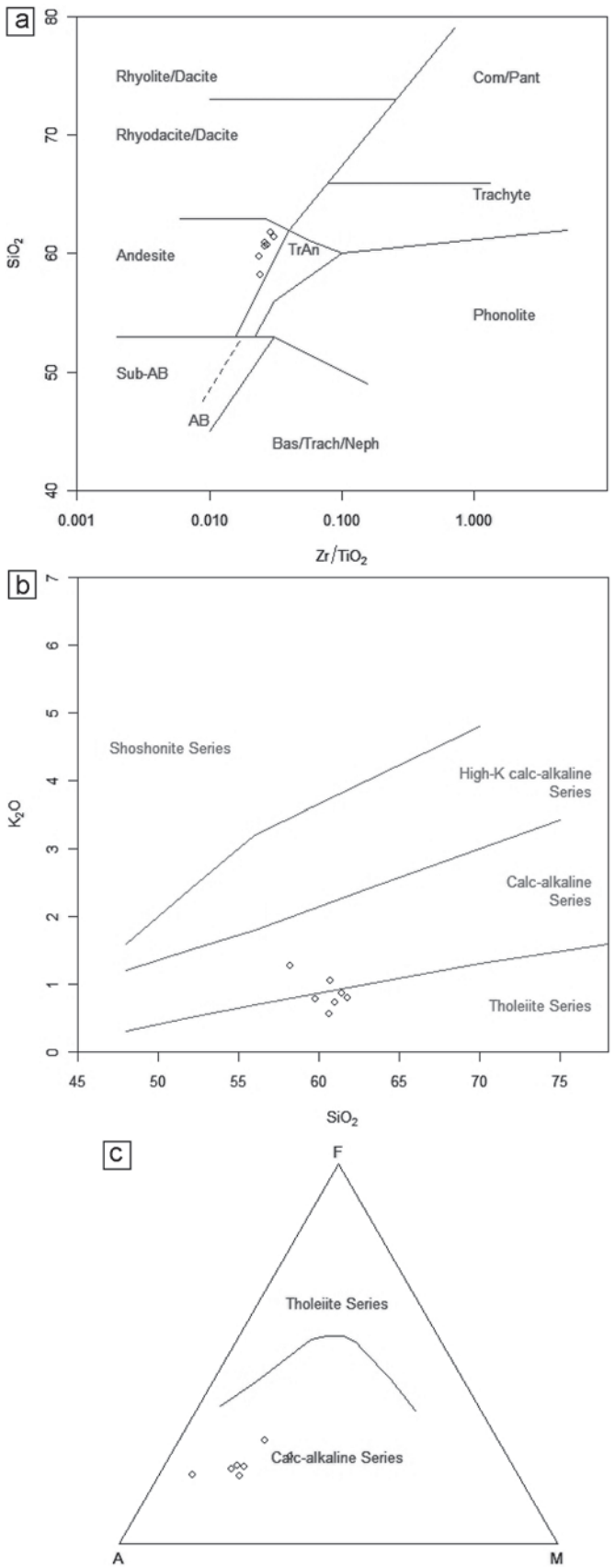

Fig. 3. Various geochemical classification diagrams showing the host rocks of the Khanlogh iron ore (a) plotting in the andesite field of the SiO_2 vs. Zr/TiO_2 plot (Winchester & Floyd 1976) (b) belonging to the calc-alkaline and tholeiitic magma series in the K_2O vs. SiO_2 diagram (Peccerillo & Taylor 1976) and (c) belonging to the calc-alkaline magma series in the MgO-FeO_{tor}-(Na_2O+K_2O) diagram (Irvine & Baragar 1971).

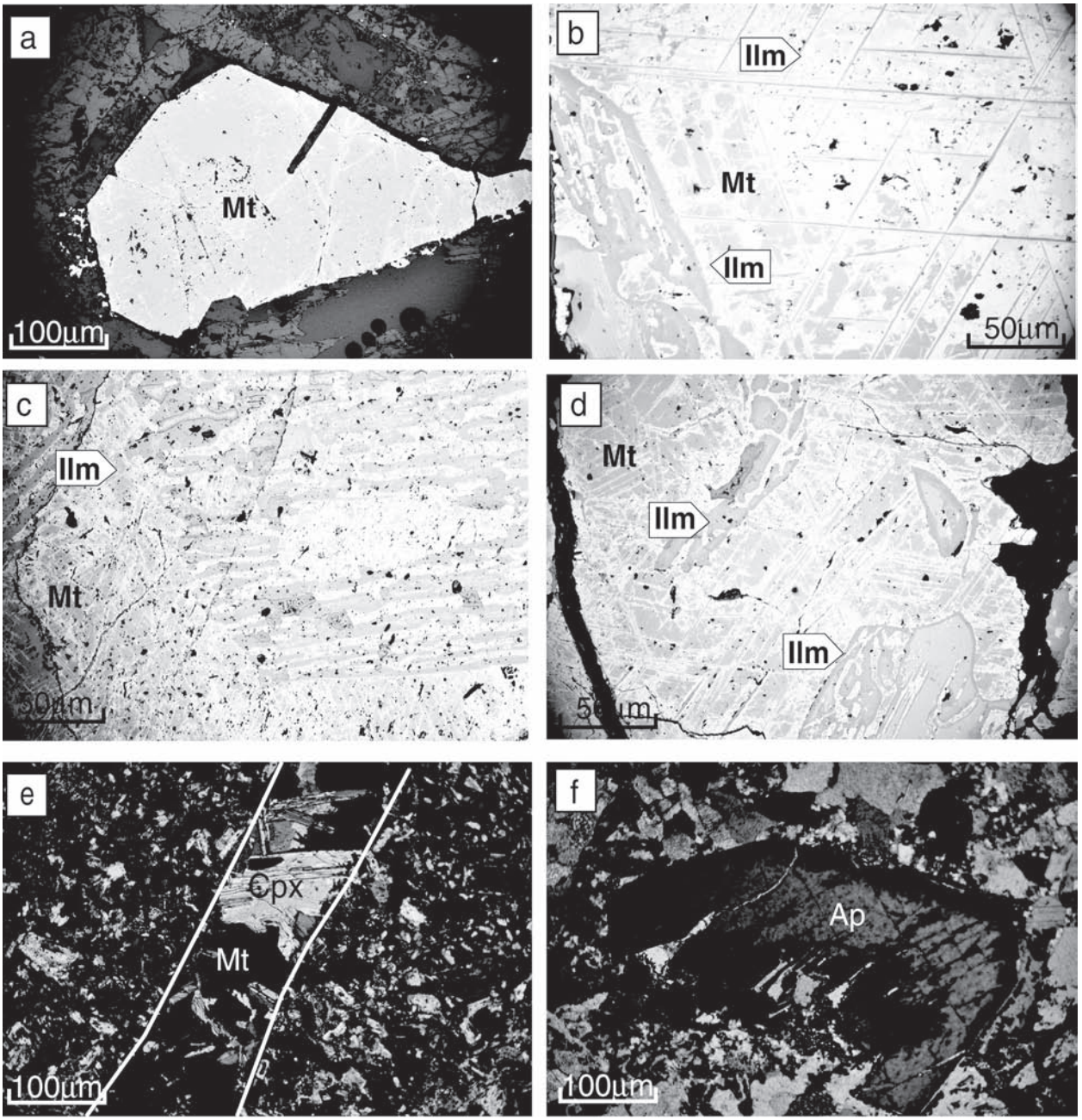

Fig. 4. Photomicrographs of the Khanlogh iron ores. (a) A magnetite crystal (Mt) altered to hematite along the cleavage plane (cross-polarized light – xpl). (b) Thin-bladed ilmenite (Ilm) with trellis and granular textures (xpl). (c) Thick-bladed ilmenite (Ilm) with sandwich texture. (d) Granular ilmenite (xpl). (e) Veinlet containing magnetite (Mt) and diopside (Cpx). (f) Apatite crystal partially altered to calcite.

The chemical analyses for major and trace elements are listed in Table 1. In the SiO_2 vs. Zr/TiO_2 bivariate plot of Winchester & Floyd (1977; Fig. 3a) the host rocks plot in the field of intermediate igneous rocks (andesite or diorite). Based upon the SiO_2 vs. K_2O bivariate (Fig. 3b) and MgO-FeO-(K_2O+Na_2O) ternary

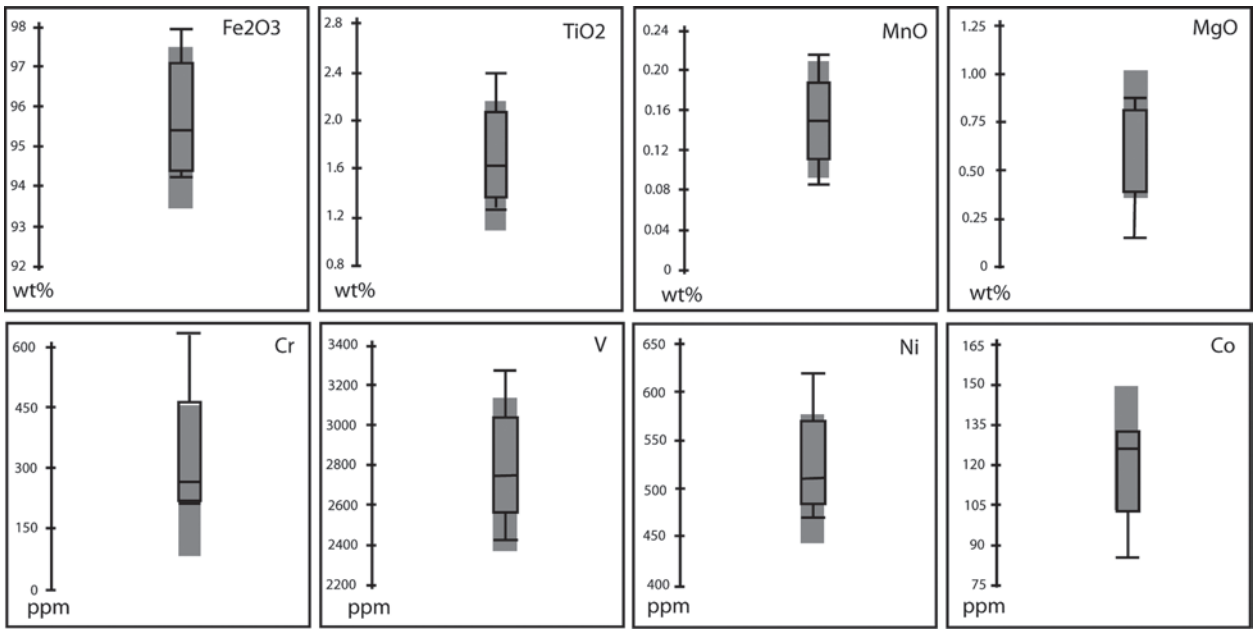

Fig. 5. Fe_2O_3, TiO_2, MnO, and MgO and Cr, V, Ni, and Co concentrations in Khanlogh magnetite ores.

plots (Fig. 3c) the host rocks belong to the calc-alkaline to tholeiitic magma series.

Alteration

Various alteration zones, including propylitic, calcic, and argillic alteration types, are observed in outcrops of the study area. The propylitic alteration zone, however, is the largest and distinguishable by the pale to dark green color imparted by green minerals such as chlorite and epidote.

Calcic alteration occurs as dark green colored haloes caused by the presence of diopside, calcite, and phlogopite in the walls of magnetite-bearing vein/veinlets and stockworks.

Argillic alteration zones are white on outcrop surfaces and in this zone feldspars are severely altered to montmorillonite and quartz.

Ore petrography

The Khanlogh iron ores developed within fractured and brecciated zones in dioritic subvolcanic host rocks. The mineralized zones extend up to 1000 meters and mineralization occurs as veins, stockworks, disseminations, and open space fillings in fault breccia zones. The Fe-bearing veins have varying thicknesses (5-100 mm), an overall NW-SE trend and dip c. 50-60° S-SW. The ores within the veins contain martitized magnetite along with clinopyroxene and apatite. Coarse solitary magnetite crystals (1-10 mm) along with clinopyroxenes are present in the stockwork zone. The fault breccia clasts have host rock compositions, vary in size from 1 mm to >5 cm and are cemented by martitized magnetite. In thin section, the magnetite crystals in the ores are fine- to coarse-grained, subhedral to euhedral showing granular and massive textures (Fig. 4a). These magnetites were martitized in supergene zones and contain exsolutions of ilmenite. Ilmenites are observed in three distinct forms within the magnetite: (1) thin-bladed with trellis texture (Fig. 4b), (2) thick-bladed with sandwich texture (Fig. 4c), and (3) fine granular grains (Fig. 4d) that are relatively more abundant and present along the margins of the magnetite crystals.

The important gangue minerals in the ores are clinopyroxene, apatite, quartz, and calcite accompanied by smaller amounts of actinolite, phlogopite, albite, and barite. Clinopyroxenes are principally diopside of varying abundance and size, subhedral to euhedral in shape and intergrown with magnetite (Fig. 4e).

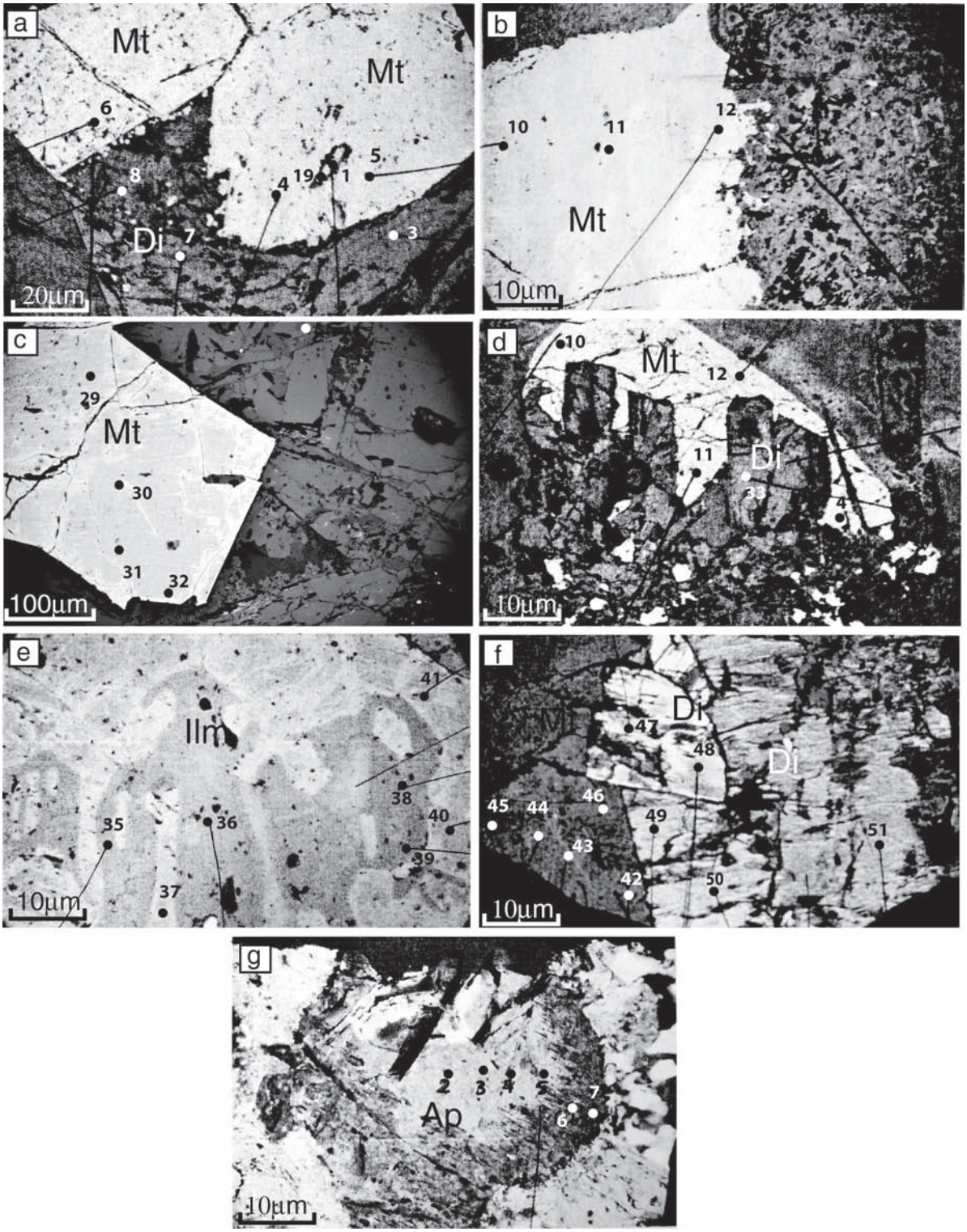

Fig. 6. Photomicrographs with EPMA points. (a) Magnetite (Mt), ilmenite (Ilm), hematite (Hem), and diopside (Di), sample 330 (ppl). (b) Magnetite (Mt), and ilmenite (Ilm) sample 330 (ppl). (c) Magnetite (Mt), sample 424 (ppl). (d) Magnetite (Mt) and diopside (Di), sample 424 (ppl). (e) Ilmenite (Ilm), and Magnetite (Mt), sample 415 (plane plorized light -ppl), (f) Magnetite (Mt) and diopside (Di), sample 415 (ppl). (g) Apatite (Ap), sample 427 (cross xpl).

Apatite occurs as fine- to coarse-grained (Fig. 4f), subhedral to euhedral crystals intimately associated with magnetite and diopside. SEM examinations reveal that they contain monazite inclusions. It is noteworthy that apatite proportions notably decrease with increasing amounts of diopside.

Bulk-rock geochemistry of the magnetite ores

The XRF analyses of the separate magnetite crystals indicate that the concentration of Mn, Al, Si, V, Zn, Cu, Ni, Co, Ti, and Mg show relatively wide concentration ranges (Fig. 5; Table 2).

Mineral chemistry of the iron ores

Electron probe micro-analyses (EPMA) of the Khanlogh iron ore samples comprise a total of 20 points on magnetite (2-4 points per individual grain), 6 points on ilmenite, 2 points on hematite, 9 points on diopside, and 6 points on apatite (Fig. 6).

Significant variation in chemical composition of the Khanlogh magnetite was observed. In general, the factors controlling the concentration values of trace elements in magnetite include (1) formation temperature, (2) concentration of elements in hydrothermal fluids, (3) sulfur fugacity (fS_2), (4) intensity of chemical reactions between fluids and host rocks (Nadoll et al. 2014). Since the subvolcanic host rocks at Khanlogh have relatively low chemical reactivity, the variation in composition of magnetite crystals may be due to the changes in composition of the hydrothermal fluids resulting from a gradual decrease in temperature during the formation of the Khanlogh ores. The main minor elements are V (V_2O_3 = 0.62 ± 0.01 wt.%), Ti (TiO_2 = 1.80 ± 1.54 wt.%), Mn (MnO = 0.17 ± 0.01 wt.%), and Mg (MgO = 0.62 ± 0.07 wt.%) (Table 3). The concentrations of the divalent (Mn, Ni, Mg, and Zn), and tri- and tetravalent cations (Al, V, Si) are very low (Table 3). The stoichiometric formula of magnetite is $Fe^{2+}_{0.94}Fe^{3+}_{1.88}O_4$ and is of $Mt_{99}Ul_{0.05}$ type. The granular ilmenites contain Mg (MgO = 3.3 wt.%), V (V_2O_3 = 1.96 wt.%), Mn (MnO = 2.6 wt.%), and the trellis ilmenite contains Mg (MgO = 0.41 wt.%), V (V_2O_3 = 1.97 wt.%), and Mn (MnO = 4.03 wt.%) (Table 4). Both granular and trellis ilmenite inclusions contain negligible amounts of Fe^{3+}. In general, the average V, Mg, and Mn-oxide concentrations in ilmenite are somewhat higher than those in magnetite. The Ti/(Ti+Fe) ratios of ilmenite and magnetite are 0.5 and 0.02, respectively and in the FeO-Fe_2O_3-TiO_2 ternary diagram they plot in the ilmenite-magnetite solid solution field (Fig. 7).

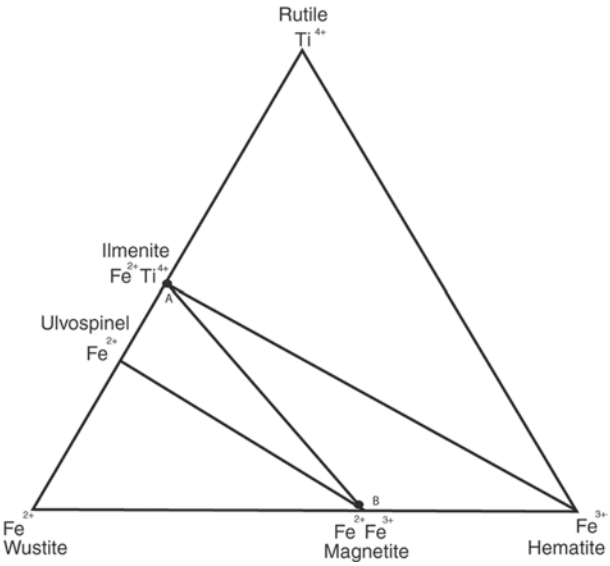

Fig. 7. Magnetite-ulvöspinel and ilmenite-hematite solid solutions in the TiO_2-FeO-Fe_2O_3 ternary system (Lindsley & Lindh 1974). Khanlogh ilmenite and magnetite compositions (filled circles) plot in the ilmenite-magnetite solid solution field.

The main minor elements in hematite are V (V_2O_3 = 0.5 to 0.06 wt.%), Ti (TiO_2 = 2 to 1.38 wt.%), Mn (MnO = 0 to 0.07 wt.%), and Mg (MgO = 0.03 to 0.05 wt.%) (Table 5).

Those coexisting clinopyroxenes that are intergrown with magnetite are mainly diopside (Di_{90-100}) with the stoichiometric formula $Ca_{0.8}Mg_{0.68}Si_{1.77}O_6$. The other minor constituent elements are Ti (TiO_2 = 0.13 wt.%) and Fe (FeO = 8.47 wt.%). Chemical zoning was not detected in individual crystals and their bulk compositions are almost uniform (Table 6). Coexisting apatite intergrown with magnetite and diopside has the stoichiometric formula $Ca_{4.6}(PO_4)_{2.92}F_{0.74}$ and contains small amounts of Ce (Ce_2O_3 = 0.85 wt.%), La (La_2O_3 = 0.36 wt.%), Na (Na_2O = 14 wt.%), S (SO_3 = 0.03 wt.%), and Th (ThO_2 < 0.4 wt.%) (Table 7).

Magnetite-ilmenite geothermometry

Ilmenite and magnetite are members of hematite-ilmenite (Fe_2O_3-$FeTiO_3$) and magnetite-ulvöspinel ($Fe^{2+}Fe^{3+}{}_2O_4$-$Fe^{2+}{}_2TiO_4$) solid solution series, respectively. Geothermometry and oxy-barometry on Fe-Ti oxides are based on temperature and oxidation-reduc-

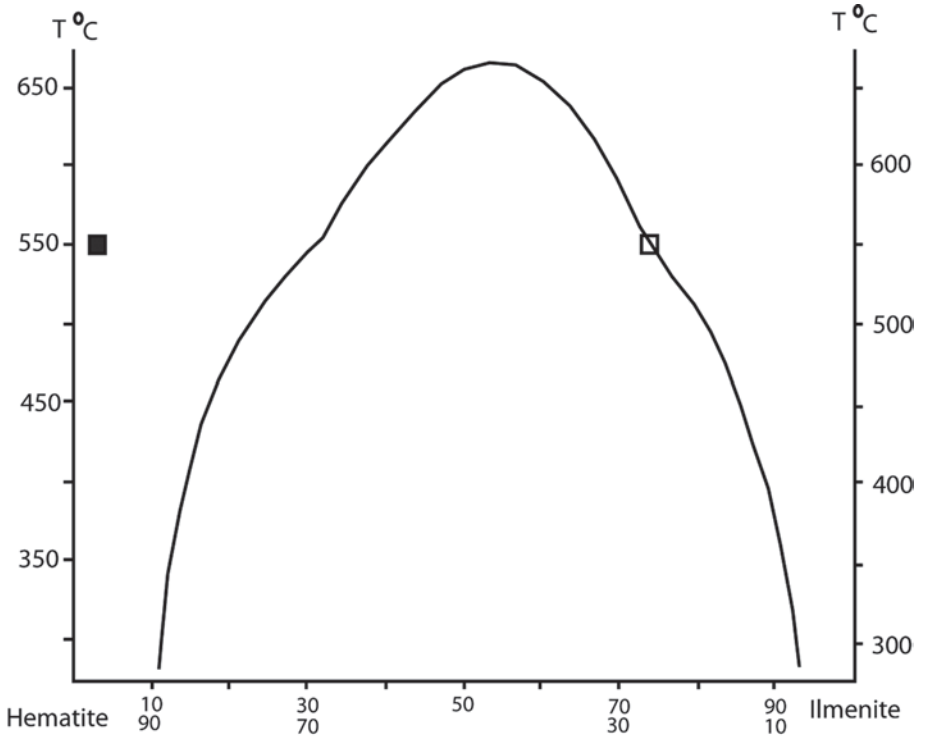

Fig. 8. Solvus diagram of the hematite-ilmenite system showing the position of the Khanlogh data points (open square Hem_{28}-Ilm_{72}, filled square Hem_{96}-Ilm_4).

tion between titano-magnetite and hematite-ilmenite in the FeO-Fe_2O_3-TiO_2 system (Buddington & Lindsley 1964). The phase relations in the hydrothermal system FeO-Fe_2O_3-TiO_2 (defined within the temperature and pressure range of 300-700 °C and 500-2000 bars) show that magnetite and rutile are stable at temperatures >550 °C while the stability fields of hematite and ilmenite are at lower temperatures (Lindh 1972). The phases Hem_{28}-Ilm_{72} and Hem_{96}-Ilm_4 plot on the solvus curve in Fig. 8 (Lindh 1972), showing that the Khanlogh iron ores were formed at temperatures of about 550 °C. According to Fig. 9 (Buddington & Lindsley 1964), the ores were formed at temperatures of around 550°C and $fO_2 \approx 10^{-18}$ atm.

Geochemistry of vanadium in magnetite-ilmenite minerals

Vanadium behaves differently with varying temperature and fO_2. Under most conditions at which magnetite and/or ilmenite are stable at high temperature, V is dominantly V^{3+} and substitutes mainly for Fe^{3+} (Schuiling & Feenstra 1980). When both magnetite and hematite are present, V^{3+} enters the crystal structure of hematite (Schuiling & Feenstra 1980). Under hydrothermal conditions within the temperature range 500-800 °C and at a pressure of 1 kbar, fO_2 is close to the hematite-magnetite buffer curve (HM) and V_2O_3 is not stable and under such conditions. V occurs as both V_2O_4 and a V^{3+}-V^{4+} mix. In this case, in fact, a portion of the V^{3+} converts to V^{4+} and substitutes for Ti^{4+} in hemo-ilmenite, ilmeno-hematite and/or rutile, and a large portion of V_2O_3 lies below the HM buffer curve (Schuiling & Feenstra 1980). The average V concentration in magnetite crystals at Khanlogh is 2805 ppm, and V is mainly concentrated in ilmenite inclusions. Vanadium also shows a good and positive correlation with Fe^{2+} (Fig. 10). On the log fO_2 -T diagram of Schuiling & Feenstra (1980) the Khanlogh magnetite-ilmenite solid solution plots close to the HM buffer curve (Fig. 11). This therefore suggests that the greater portion of vanadium in the Khanlogh iron ores is present in the form of V^{4+} replacing Ti^{4+} in ilmeno-hematite coexisting with magnetite (note that the ionic radius of Ti^{4+} = 0.64 Å and that of V^{4+} = 0.61 Å).

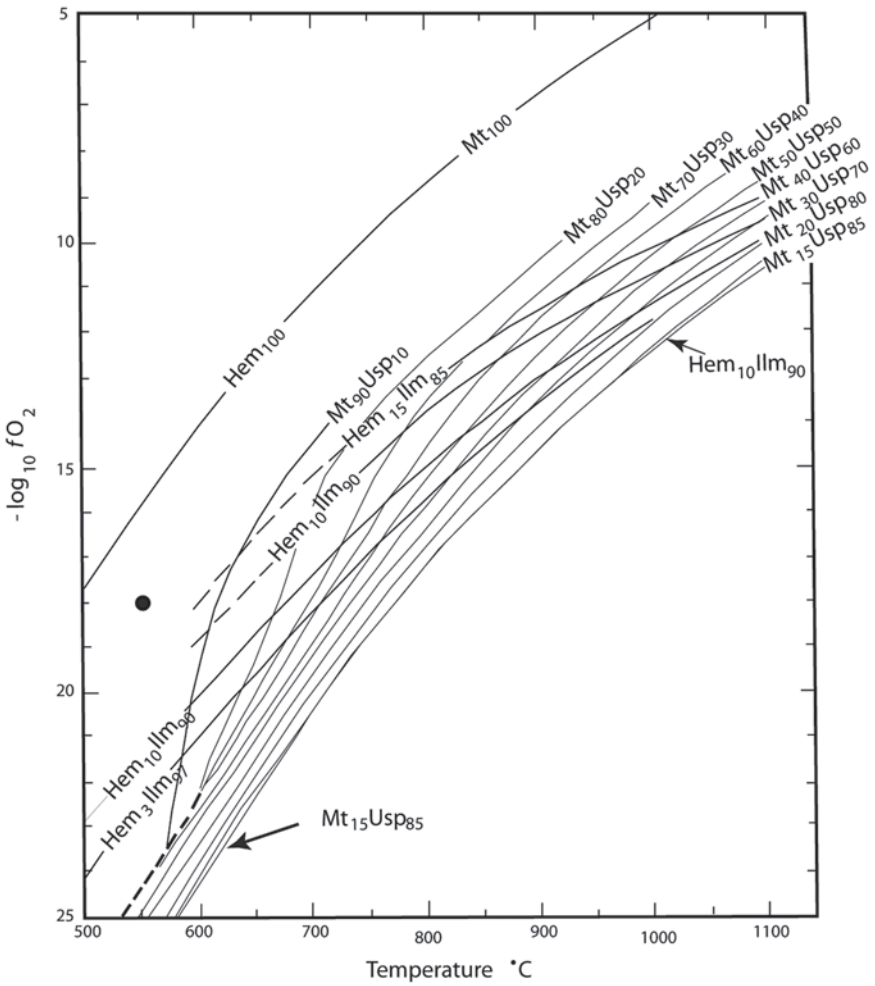

Fig. 9. Geothermometry diagram (Buddington & Lindsley 1964) showing the position of Khanlogh data points (filled circle).

Formation of the Khanlogh iron ores

The high phosphorus concentration in ore-forming fluids is a major controlling factor for hemo-magnetite and magnetite mineralization (Kärkkäinen & Appelqvist 1999). Magnetite crystallization ceases in Fe- and Ti-bearing magmas with high phosphorus contents (P_2O_5 > 1%) and, instead, $Fe^{3+}(PO_4)^{2-}$ complexes form (Toplis et al. 1994). At Khanlogh, iron was likely transported as $FeCl^-$ and $Fe^{3+}(PO_4)^{2-}$ complexes and Ti by anions such as CO_3^{2-}, F^-, and Cl^- (Ryzhenko et al. 2006). The presence of apatite-magnetite intergrowths indicates high P and Fe contents of the ore-forming fluids (Najafzadeh Tehrani et al. 2016). The analyses suggest that the mineralization of Fe, Ti, and P at Khanlogh was associated with calc-alkaline-tholeiitic magmatism of the Sabzevar-Quchan magmatic arc, and was concurrent with the formation of diopside and albite in sodic-calcic alteration zones at temperatures of approximately 550 °C.

Conclusions

The magnetite-apatite mineralization at Khanlogh occurs as veins, disseminations, stockworks, and open space fillings in brecciated zones in subvolcanic host rocks of intermediate composition. The mineralized zones contain magnetite, apatite and diopside, and the magnetite crystals have exsolved inclusions of ilmenite. V^{4+} replaced Ti^{4+} in the ilmenite crystal structure resulting in higher V contents relative to those in magnetite in the same grain. Magnetite-hemoilmentite solid

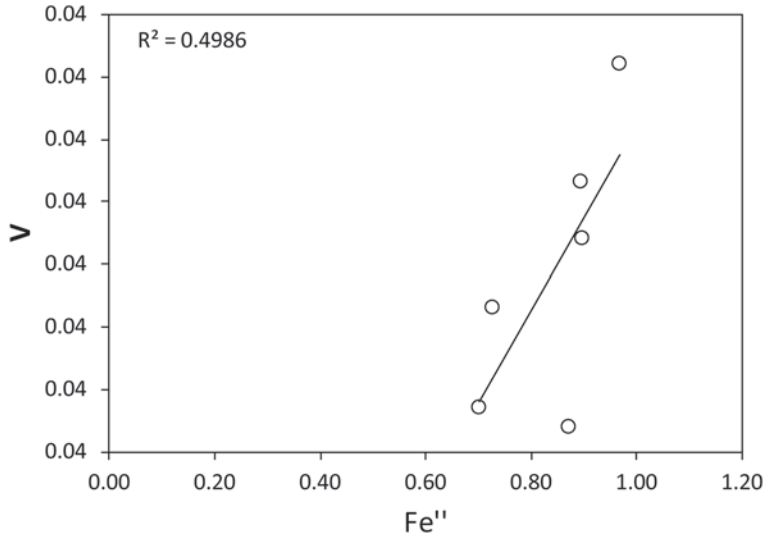

Fig. 10. Correlation of vanadium with Fe^{2+} in ilmenite inclusions.

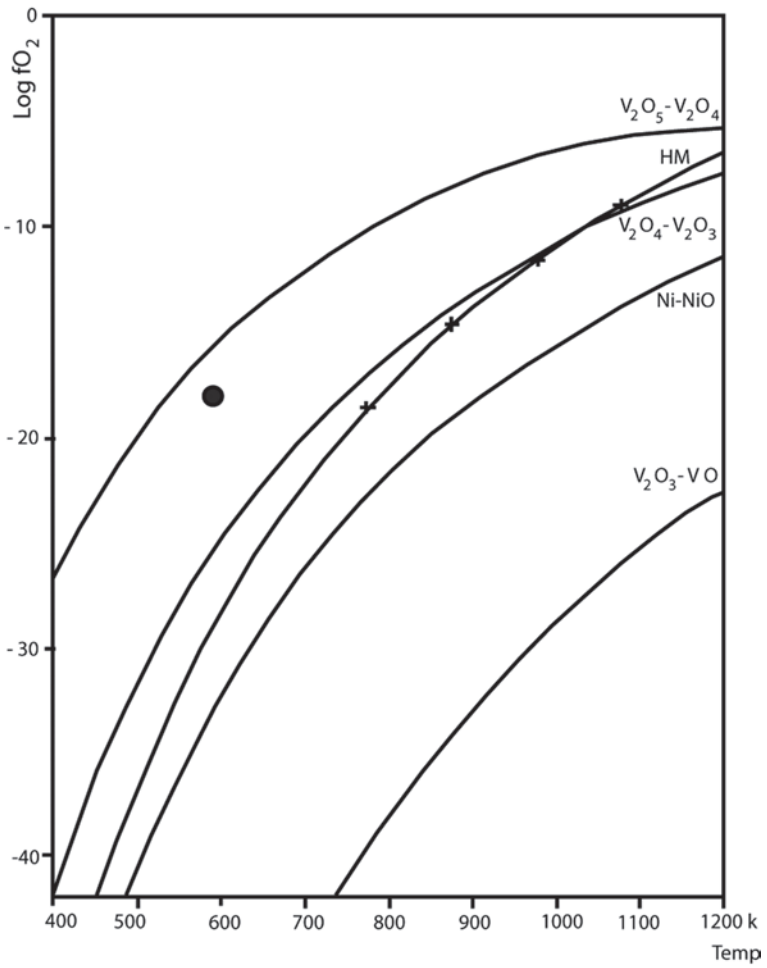

Fig. 11. Bivariate of temperature versus fO_2 plot showing the stability fields of the various oxidation states of vanadium (Schuiling & Feenstra 1980). Shown also is the position of the Khanlogh data, which plot close to HM buffer curve.

solution geothermometry indicates that mineralization occurred at about 550 °C and fO_2=10^{-18} atm. The potential source of the hot hydrothermal fluids with high content of Fe, Ti, P, and Cl was calc-alkaline-tholeiitic magmatism in the Sabzevar-Quchan magmatic arc.

Acknowledgments

The authors would like to express their thanks to Prof. Inaki Yusta of the Science and Technology Faculty of Bilbao University, Spain for conducting all XRF analyses. We would like to extend our appreciation to the Research Bureau of the University of Tabriz and the Iranian Research Center of Mineral Materials for providing financial support for this study. Our thanks are further expressed to Dr. Martin Timmerman for his valuable suggestions and editorial assistance, and also to Dr. Jaayke Knipping (University of Michigan) for reviewing and making comments on this manuscript.

References

Alavi, M. (1992): Thrust tectonics of the Binalood region, NE Iran. – Tectonics, **11**: 360-370.

Buddington, A. & Lindsley, D. (1964): Iron-titanium oxide minerals and synthetic equivalents. – Journal of Petrology, **5**: 310-357.

Charlier, B., Namur, O., Bolle, O., Latypov, R. & Duchesne, J.-C. (2015): Fe-Ti-V-P ore deposits associated with Proterozoic massif-type anorthosites and related rocks. – Earth-Science Reviews, **141**: 56-81.

Charlier, B., Skår, Ø., Korneliussen, A., Duchesne, J.-C. & Vander Auwera, J. (2007): Ilmenite composition in the Tellnes Fe-Ti deposit, SW Norway: fractional crystallization, postcumulus evolution and ilmenite-zircon relation. – Contributions to Mineralogy and Petrology, **154**: 119-134.

Clark, A.H. & Kontak, D.J. (2004): Fe-Ti-P oxide melts generated through magma mixing in the Antauta subvolcanic center, Peru: implications for the origin of nelsonite and iron oxide-dominated hydrothermal deposits. – Economic Geology, **99**: 377-395.

Dare, S.A.S., Barnes, S.-J., Beaudoin, G., Méric, J., Boutroy E. & Potvin-Doucet, C. (2014): Trace elements in magnetite as petrogenetic indicators. – Mineralium Deposita, **49**: 785-796.

Dupuis, C. & Beaudoin, G. (2011): Discriminant diagrams for iron oxide trace element fingerprinting of mineral deposit types. – Mineralium Deposita, **46**: 319-335.

Frost, B. & Lindsley, D.H. (1991): Occurrence of iron-titanium oxides in igneous rocks. – Reviews in Mineralogy and Geochemistry, **25**: 433-468.

Ghiorso, M.S. & Sack, O. (1991): Fe-Ti oxide geothermometry: thermodynamic formulation and the estimation of intensive variables in silicic magmas. – Contributions to Mineralogy and Petrology, **108**: 485-510.

Irvine, T. & Baragar, W. (1971): A guide to the chemical classification of the common volcanic rocks. – Canadian Journal of Earth Sciences, **8**: 523-548.

Kärkkäinen, N. & Appelqvist, H. (1999): Genesis of a low-grade apatite-ilmenite-magnetite deposit in the Kauhajärvi gabbro, western Finland. – Mineralium Deposita, **34**: 754-769.

Lattard, D., Sauerzapf, U. & Käsemann, M. (2005): New calibration data for the Fe-Ti oxide thermo-oxybarometers from experiments in the Fe-Ti-O system at 1 bar, 1,000-1,300 C and a large range of oxygen fugacities. – Contributions to Mineralogy and Petrology, **149**: 735-754.

Lindh, A. (1972): A hydrothermal investigation of the system FeO, Fe_2O_3, TiO_2. – Lithos, **5**: 325-343.

Lindsley, D.H. & Lindh, A. (1974): A hydrothermal investigation of the system FeO-Fe_2O_3-TiO_2: A discussion with new data. – Lithos, **7**: 65-68.

Mücke, A. (2003): Magnetite, ilmenite and ulvite in rocks and ore deposits: petrography, microprobe analyses and genetic implications. – Mineralogy and Petrology, **77**: 215-234.

Nabavi, M. (1976): An introduction to the geology of Iran. – Geological Survey of Iran (in Farsi).

Nadoll, P., Angerer, T., Mauk, J.L., French, D. & Walshe, J. (2014): The chemistry of hydrothermal magnetite: a review. – Ore Geology Reviews, **61**: 1-32.

Najafzadeh Tehrani, P., Calagari, A.A., Velasco Roldan, F., Simmonds, V. & Siahcheshm, V. (2016): Magnetite-apatite mineralization in Khanlogh iron deposit, northwest of Neyshaboor, NE Iran. – European European Geosciences Union (EGU) meeting abstract. Austria, Vienna.

Oliver, G.J. (1978): Ilmenite-magnetite geothermometry and oxygen barometry in granulite and amphibolite facies gneisses from Doubtful Sound, Fiorland, New Zealand. – Lithos, **11**: 147-153.

Peccerillo, A. & Taylor, S. R. (1976): Geochemistry of Eocene calc-alkaline volcanic rocks from the Kastamonu area, northern Turkey. – Contributions to Mineralogy and Petrology, **58**: 63-81.

Philpotts, A. (1967): Origin of certain iron-titanium oxide and apatite rocks. – Economic Geology, **62**: 303-315.

Pouchou, J.L. & Pichoir, J. (1984): A new model for quantitative x-ray microanalysis. Part I: application to the analysis of homogeneous samples. – Rech. Aerosp. **3**: 167-192.

Ramezani, J. & Tucker, R.D. (2003): The Saghand region, Central Iran: U-Pb geochronology, petrogenesis and implications for Gondwana tectonics. – American Journal of Science, **303**: 622-665.

Ryzhenko, B., Kovalenko, N. & Prisyagina, N. (2006): Titanium complexation in hydrothermal systems. – Geochemistry International, **44**: 879-895.

Schuiling, R. & Feenstra, A. (1980): Geochemical behaviour of vanadium in iron-titanium oxides. – Chemical Geology, **30**: 143-150.

She, Y.-W., Song, X.-Y., Yu, S.-Y. & He, H.-L. (2015): Variations of trace element concentration of magnetite and ilmenite from the Taihe layered intrusion, Emeishan large igneous province, SW China: Implications for magmatic fractionation and origin of Fe-Ti-V oxide ore deposits. – Journal of Asian Earth Sciences, **113**: 1117-1131.

Spies, O., Lensch, G. & Mihem. A. (1983): Chemistry of

post-ophiolithic tertiary volcanic between Sabzevar and Quchan, NE Iran. – In: Almassi. A. (Ed.): Geodynamic project (geotravers) in Iran. Geological Survey of Iran, Tehran; 247-266.

Toplis, M.J., Dingwell, D.B. & Libourel, G. (1994): The effect of phosphorus on the iron redox ratio, viscosity, and density of an evolved ferro-basalt. – Contributions to Mineralogy and Petrology, **117**: 293-304.

Whalen, J.B. & Chappell, B.W. (1988): Opaque mineralogy and mafic mineral chemistry of I-and S-type granites of the Lachlan fold belt, southeast Australia. – American Mineralogist, **73**, 281-296.

Winchester, J. & Floyd, P. (1977): Geochemical discrimination of different magma series and their differentiation products using immobile elements. – Chemical Geology, **20**: 325-343.

Zarei, A., Malekzadeh Shafaroudi, A. & Karimpour, M.H. (2016): Geochemistry and genesis of iron-apatite in Khanlogh deposit, Estern Canozoic Quchan-Sabzevar magmatic arc, NE Iran. – Acta Geologica Sinica (english version), **90**: 121-137.

Manuscript received: May 24th, 2016.
Revised version accepted by the Potsdam editor: August 1st, 2016.

Addresses of the authors:

Parvin Najafzadeh Tehrani (corresponding author), Ali Asghar Calagari, Kamal Siahcheshm, Department of Geology, Faculty of Natural Sciences, University of Tabriz, 5166616471, Tabriz, Iran.
e-mail: par_najafzadeh@tabrizu.ac.ir and parvin_tehranii@yahoo.com

Francisco Velasco Roldan, Department of Mineralogy and Petrology, Faculty of Science and Technology, University of Bilbao, UPV/EHU, 48080 Bilbao, Spain.
e-mail: francisco.velasco@ehu.es

Vartan Simmonds, Research Institute for Fundamental Sciences, University of Tabriz, 5166876393, Tabriz, Iran.
e-mail: simmonds_vartan@yahoo.co.uk

Appendix

Table 1. Major, minor, and trace element XRF analyses of the host rocks to the Khanlogh iron ores. b.d. = below detection limit, n.a. = not analyzed.

Sample	330h	412	418	433	440	448	449h
SiO_2 (wt%)	61.44	58.24	60.66	60.97	60.73	59.75	61.8
Al_2O_3	14.75	14.49	15.42	15.29	14.4	14.26	14.87
Fe_2O_3	2.09	2.99	2.11	1.57	2.31	2.75	1.84
MnO	0.03	0.07	0.05	0.04	0.05	0.04	0.03
MgO	1.74	1.95	1.57	0.59	1.7	2.99	1.75
CaO	4.12	4.61	5.02	4.7	5.49	4.01	3.9
Na_2O	4.86	3.98	5.74	5.03	5.33	4.59	5.17
K_2O	0.87	1.28	0.56	0.73	1.06	0.77	0.79
TiO_2	0.24	0.22	0.25	0.27	0.24	0.25	0.24
P_2O_5	0.03	0.08	0.03	0.08	0.03	0.03	0.03
As (ppm)	7.93	7.57	31.06	53.29	6.65	24.8	6.97
Ba	216.93	220.75	125.86	209.66	145.4	203.12	208.86
Co	b.d.	10.81	5.7	6.02	3.68	9.09	3.25
Cu	198.95	52.32	197.21	62.41	178.38	61.04	159.68
Ni	27.94	19.67	47.5	28.17	15.42	89.31	14.85
Pb	23.31	12.43	18.58	25.01	24.14	14.31	25.34
Rb	n.d.	n.d.	5	34	n.d.	n.d.	n.d.
S	190.21	176.63	131.45	129.59	123.27	130.24	168.07
Sr	318.32	474.53	355.55	329.43	373.23	393.55	302.68
Y	6.62	6.16	1.08	b.d.	11.73	b.d.	11.2
Zn	32.53	26.45	26.24	38.61	17.24	23.82	13.19
Zr	74.4	53.97	65.44	72.17	64.55	60.1	69.15
W	b.d.	b.d.	b.d.	b.d.	14.46	b.d.	4.16
V	83.99	88	78.7	70.91	70.5	79.91	71.94
Cr	114.95	390.92	40.07	0.81	34.01	93.48	27.36
Nb	0.31	b.d.	0.25	1.51	0.66	6.26	b.d.

Table 2. Major, minor, and trace element XRF analyses for magnetites of the Khanlogh iron ores.

Sample	KH330	KH415	KH428	KH447
SiO_2 (wt%)	2.38	1.96	1.27	0.30
Al_2O_3	1.21	0.59	0.55	0.48
Fe_2O_3	94.75	96.21	94.27	97.95
MnO	0.22	0.14	0.16	0.09
MgO	0.63	0.88	0.75	0.16
CaO	0.34	1.14	1.38	0.36
Na_2O	0.20	0.00	0.01	0.00
K_2O	0.04	0.00	0.00	0.00
TiO_2	1.74	1.27	2.40	1.52
P_2O_5	0.01	0.01	0.01	b.d.
As (ppm)	27.64	24.58	31.24	21.14
Ba	540.55	553.23	496.88	544.73
Co	120.51	133.21	132.41	85.58
Cu	1125.09	1420.76	541.28	688.56
Ni	501.61	621.36	520.62	470.29
Pb	129.89	120.00	119.57	98.41
Rb	89.97	73.33	76.73	62.27
S	98.91	152.52	137.47	708.16
Sr	16.35	6.60	6.71	5.93
Y	6.56	b.d.	b.d.	b.d.
Zn	252.46	163.54	118.79	126.96
Zr	b.d.	b.d.	b.d.	b.d.
W	11.95	33.79	19.31	12.32
V	2429.40	3280.31	2702.96	2807.05
Cr	215.19	634.17	298.23	240.05
Nb	0.08	6.84	15.66	7.39

Table 3. Electron probe micro-analyses of magnetite crystals for Khanlogh iron ore samples.

Sample	330	330	330	330	330	424	424	424	424	424	424	424	424	415	415	415	415	415	415
	4	5	6	10	12	4	10	11	12	29	30	31	32	40	41	42	43	44	45	46
Point	Magne-tite	Magne-tite	Magne-tite	Magne-tite	Magne-tite	Magne-tite	Magne-tite	Magne-tite	Magne-tite	Magne-tite	Magne-tite	Magne-tite	Magne-tite	Magne-tite	Magne-tite	Magne-tite	Magne-tite	Magne-tite	Magne-tite	Magne-tite
SiO_2	0.30	0.37	0.34	0.34	0.29	0.25	0.61	0.24	0.22	0.30	0.30	0.43	0.37	0.24	0.25	0.27	0.23	0.24	0.25	0.29
FeO	29.93	28.27	30.32	30.39	29.61	30.28	29.23	27.92	29.75	28.34	30.39	30.22	30.56	29.96	29.98	29.84	30.02	29.90	29.89	30.40
Fe_2O_3	66.03	66.76	66.89	67.04	65.31	66.79	64.47	65.95	65.64	62.53	67.05	66.67	67.41	66.10	66.15	65.82	66.23	65.97	65.95	67.07
Al_2O_3	0.33	0.40	0.29	0.30	0.33	0.08	2.04	0.49	0.74	0.27	0.26	1.07	0.44	0.27	0.25	0.50	0.27	0.31	0.33	0.31
CaO	0.00	0.01	0.00	0.02	0.00	0.03	0.01	0.00	0.01	0.00	0.03	0.04	0.03	0.00	0.00	0.01	0.02	0.03	0.00	0.00
MgO	0.63	0.56	0.54	0.76	0.73	0.58	0.40	1.53	0.26	0.98	0.35	0.48	0.36	0.84	0.69	0.73	0.33	0.66	0.68	0.33
TiO_2	1.77	1.89	1.44	1.93	2.03	0.28	2.10	2.07	0.99	6.48	0.17	0.64	0.70	1.99	1.96	2.11	1.94	1.92	2.07	1.29
MnO	0.35	0.27	0.34	0.26	0.25	0.10	0.08	0.08	0.04	0.20	0.01	0.07	0.05	0.19	0.13	0.25	0.17	0.21	0.19	0.07
ZnO	0.06	0.03	0.09	0.01	0.01	0.00	0.00	0.02	0.00	0.00	0.07	0.00	0.06	0.00	0.00	0.00	0.05	0.03	0.16	0.16
Cr_2O_3	0.00	0.02	0.00	0.04	0.00	0.00	0.00	0.03	0.06	0.01	0.03	0.01	0.01	0.00	0.04	0.00	0.06	0.04	0.00	0.01
Na_2O	0.06	0.00	0.06	0.00	0.00	0.02	0.06	0.04	0.00	0.00	0.05	0.13	0.04	0.02	0.00	0.00	0.00	0.04	0.00	0.00
NiO	0.02	0.03	0.02	0.05	0.04	0.01	0.09	0.08	0.05	0.01	0.07	0.10	0.16	0.11	0.02	0.07	0.01	0.10	0.10	0.02
V_2O_3	0.58	0.41	0.46	0.50	0.43	0.66	0.64	0.62	0.65	0.88	0.66	0.64	0.71	0.73	0.70	0.60	0.66	0.66	0.65	0.57
Total	100.06	99.03	100.80	101.64	99.04	99.07	99.71	99.07	98.40	100.00	99.44	100.50	100.90	100.46	100.18	100.18	100.00	100.11	100.27	100.54
								Formula per 4 Oxygen (all Fe as FeO)												
Si	0.01	0.01	0.01	0.01	0.01	0.01	0.02	0.01	0.01	0.01	0.01	0.02	0.01	0.01	0.01	0.01	0.01	0.01	0.01	0.01
Fe''	0.95	0.90	0.96	0.95	0.95	0.98	0.92	0.89	0.96	0.88	0.98	0.95	0.97	0.95	0.95	0.94	0.95	0.95	0.95	0.96
Fe'''	1.88	1.92	1.90	1.88	1.88	1.94	1.82	1.88	1.91	1.75	1.94	1.89	1.92	1.88	1.88	1.87	1.89	1.88	1.88	1.91
Al	0.01	0.02	0.01	0.01	0.01	0.00	0.09	0.02	0.03	0.01	0.01	0.05	0.02	0.01	0.01	0.02	0.01	0.01	0.01	0.01
Ca	0.00	0.00	0.00	0.00	0.00	0.00	0.00	0.00	0.00	0.00	0.00	0.00	0.00	0.00	0.00	0.00	0.00	0.00	0.00	0.00
Mg	0.04	0.03	0.03	0.04	0.04	0.03	0.02	0.09	0.01	0.05	0.02	0.03	0.02	0.05	0.04	0.04	0.02	0.04	0.04	0.02
Ti	0.05	0.05	0.04	0.05	0.06	0.01	0.06	0.06	0.03	0.18	0.01	0.02	0.02	0.06	0.06	0.06	0.06	0.05	0.06	0.04
Mn	0.01	0.01	0.01	0.01	0.01	0.00	0.00	0.00	0.00	0.01	0.00	0.00	0.00	0.01	0.00	0.01	0.01	0.01	0.01	0.00
Zn	0.00	0.00	0.00	0.00	0.00	0.00	0.00	0.00	0.00	0.00	0.00	0.00	0.00	0.00	0.00	0.00	0.00	0.00	0.00	0.00
Cr	0.00	0.00	0.00	0.00	0.00	0.00	0.00	0.00	0.00	0.00	0.00	0.00	0.00	0.00	0.00	0.00	0.00	0.00	0.00	0.00
Na	0.00	0.00	0.00	0.00	0.00	0.00	0.00	0.00	0.00	0.00	0.00	0.00	0.00	0.00	0.00	0.00	0.00	0.00	0.00	0.00
Ni	0.00	0.00	0.00	0.00	0.00	0.00	0.00	0.00	0.00	0.00	0.00	0.00	0.00	0.00	0.00	0.00	0.00	0.00	0.00	0.00
V	0.02	0.01	0.01	0.01	0.01	0.02	0.02	0.02	0.02	0.03	0.02	0.02	0.02	0.02	0.02	0.02	0.02	0.02	0.02	0.02
Ulv	0.05	0.06	0.04	0.06	0.06	0.01	0.06	0.06	0.03	0.19	0.01	0.02	0.02	0.06	0.06	0.06	0.06	0.06	0.06	0.06
Mt	99.95	99.94	99.96	99.94	99.94	99.99	99.94	99.94	99.97	99.81	99.99	99.98	99.98	99.94	99.94	99.40	99.94	99.94	99.94	99.94
Ti/Fe+Ti	0.02	0.02	0.01	0.02	0.02	0.00	0.02	0.02	0.01	0.06	0.00	0.01	0.01	0.02	0.02	0.02	0.02	0.02	0.02	0.01

Table 4. Electron probe micro-analysis compositions of ilmenite exsolved inclusions (trellis and granular) in Khanlogh ore magnetites.

Sample	415	415	415	415	415	330
Point	35 Ilm granular	36 Ilm granular	37 Ilm granular	38 Ilm granular	39 Ilm granular	19 Ilm trellis
SiO_2	0.17	0.20	0.23	0.19	0.20	0.44
FeO	33.78	42.82	34.98	41.44	42.98	42.35
Fe_2O_3	9.39	0.00	9.72	0.00	0.00	0.00
Al_2O_3	0.01	0.03	0.01	0.02	0.00	0.05
CaO	0.00	0.00	0.00	0.02	0.00	0.29
MgO	2.98	3.41	3.40	3.59	3.26	0.41
TiO_2	48.12	48.87	47.52	49.32	48.76	44.31
MnO	2.49	2.92	1.17	2.90	3.63	4.03
ZnO	0.21	0.21	0.05	0.15	0.00	0.02
Cr_2O_3	0.01	0.00	0.02	0.02	0.00	0.00
Na_2O	0.00	0.00	0.00	0.01	0.02	0.00
NiO	0.02	0.01	0.02	0.03	0.00	0.00
V_2O_3	1.89	2.06	1.97	1.86	2.02	1.97
Total	99.06	100.52	99.09	99.54	100.87	93.88
Formula per 3 Oxygen (all Fe as FeO)						
Si	0.00	0.00	0.01	0.00	0.00	0.01
Fe''	0.70	0.90	0.73	0.87	0.90	0.97
Fe'''	0.18	0.00	0.18	0.00	0.00	0.00
Al	0.00	0.00	0.00	0.00	0.00	0.00
Ca	0.00	0.00	0.00	0.00	0.00	0.01
Mg	0.11	0.13	0.13	0.13	0.12	0.02
Ti	0.90	0.92	0.89	0.93	0.92	0.91
Mn	0.05	0.06	0.02	0.06	0.08	0.09
Zn	0.00	0.00	0.00	0.00	0.00	0.00
Cr	0.00	0.00	0.00	0.00	0.00	0.00
Na	0.00	0.00	0.00	0.00	0.00	0.00
Ni	0.00	0.00	0.00	0.00	0.00	0.00
V	0.04	0.04	0.04	0.04	0.04	0.04
Ilm	75.93	72.91	75.74	73.61	71.36	19.48
Hem	24.07	27.09	24.26	26.39	28.64	80.52
Ti/TiFe	0.51	0.51	0.49	0.52	0.51	0.48

Table 5. Electron probe micro-analysis compositions of hematite in Khanlogh ore magnetites

Sample	**330**	**330**
Point	11	1
	hematite	exsolved ilm+mt
	hem	hem
SiO_2	0.28	0.92
FeO(t)	86.59	85.48
Al_2O_3	0.38	0.26
CaO	0.02	0.21
MgO	0.03	0.05
TiO_2	2.00	1.39
MnO	0.00	0.08
ZnO	0.02	0.07
Cr_2O_3	0.02	0.02
Na_2O	0.00	0.08
NiO	0.00	0.11
V_2O_3	0.56	0.07
Total	89.91	89.91

Table 6. EPMA compositions of diopside intergrown with magnetite in Khanlogh iron ore samples.

Sample	**330**	**330**	**330**	**424**	**415**	**415**	**415**	**415**	**415**
Point	Pt 3	Pt 7	Pt 8	Pt 33	Pt 47	pt 48	pt 49	pt 50	pt 51
SiO_2	54.25	53.95	54.00	54.22	51.85	51.03	52.54	52.24	51.53
TiO_2	0.10	0.19	0.18	0.17	0.07	0.17	0.06	0.13	0.14
Al_2O_3	0.25	0.47	0.41	0.41	2.00	0.43	0.14	0.16	0.81
Cr_2O_3	0.00	0.00	0.02	0.00	0.00	0.00	0.01	0.06	0.03
FeO	8.23	9.04	8.32	9.00	8.44	8.83	7.93	7.89	8.54
MnO	0.24	0.21	0.16	0.22	0.14	0.13	0.18	0.14	0.15
MgO	14.67	13.80	13.81	13.71	13.40	13.43	13.17	13.39	13.29
CaO	20.68	21.07	21.09	21.00	23.21	23.23	23.71	23.92	23.36
Na_2O	0.75	1.19	1.05	0.99	0.63	0.92	0.57	0.57	0.82
K_2O	0.01	0.00	0.02	0.00	0.01	0.00	0.00	0.00	0.01
Totals	99.18	99.92	99.07	99.72	99.76	98.18	98.29	98.50	98.69
Formula per 6 Oxygen (all Fe as FeO)									
Si	1.81	1.79	1.81	1.81	1.72	1.72	1.78	1.76	1.73
Ti	0.14	0.14	0.14	0.14	0.14	0.14	0.14	0.14	0.14
Al	0.01	0.02	0.02	0.02	0.08	0.02	0.01	0.01	0.03
Fe^{+3}	0.17	0.23	0.19	0.19	0.23	0.25	0.22	0.22	0.24
Cr^{+3}	0.00	0.00	0.00	0.00	0.00	0.00	0.00	0.00	0.00
Fe^{+2}	0.06	0.02	0.04	0.06	0.00	0.00	0.00	0.00	0.00
Mn	0.26	0.26	0.26	0.26	0.26	0.27	0.27	0.27	0.27
Mg	0.73	0.68	0.69	0.68	0.66	0.68	0.66	0.67	0.67
Ca	0.74	0.75	0.76	0.75	0.83	0.84	0.86	0.86	0.84
Na	0.05	0.08	0.07	0.06	0.04	0.06	0.04	0.04	0.05
K	0.03	0.03	0.03	0.03	0.03	0.03	0.03	0.03	0.03
H	0.00	0.00	0.00	0.00	0.00	0.00	0.00	0.00	0.00
Wo	48.37	51.56	50.93	50.17	55.46	55.43	56.41	56.22	55.82
En	47.73	46.98	46.39	45.59	44.54	44.57	43.59	43.78	44.18
Fs	3.90	1.46	2.68	4.24	0.00	0.00	0.00	0.00	0.00
%di	92.45	96.98	94.54	91.48	100.00	100.00	100.00	100.00	100.00

Table 7. EPMA compositions of apatites intergrown with magnetite in Khanlogh iron ore samples.

Sample	**427**	**427**	**427**	**427**	**427**	**427**
Point	**2**	**3**	**4**	**5**	**6**	**7**
CaO	51.20	50.84	52.13	52.78	52.38	52.46
Na_2O	0.14	0.19	0.11	0.13	0.13	0.15
MnO	0.08	0.05	0.04	0.05	0.05	0.05
FeO	0.17	0.20	0.16	0.14	0.20	0.13
La_2O_3	0.34	0.36	0.33	0.31	0.41	0.40
Ce_2O_3	0.75	0.82	0.73	0.80	0.92	1.09
Pr_2O_3	0.13	0.17	0.20	0.15	0.15	0.21
Nd_2O_3	0.37	0.38	0.30	0.27	0.34	0.32
P_2O_5	42.87	42.09	40.48	42.47	41.82	42.58
SiO_2	n.d.	n.d.	n.d.	n.d.	n.d.	n.d.
Cl	1.24	1.55	2.06	2.12	2.03	1.10
F	3.65	2.56	2.66	2.32	2.65	3.36
Total	100.94	99.22	99.20	101.54	101.07	101.85
O=F,Cl	1.82	1.43	1.59	1.45	1.57	1.66
Total	99.12	97.79	97.61	100.08	99.50	100.18
Ca	8.93	9.06	9.40	9.24	9.24	9.12
Na	0.04	0.06	0.04	0.04	0.04	0.05
Mn	0.01	0.01	0.01	0.01	0.01	0.01
Fe	0.02	0.03	0.02	0.02	0.03	0.02
La	0.02	0.02	0.02	0.02	0.02	0.02
Ce	0.04	0.05	0.04	0.05	0.06	0.06
Pr	0.01	0.01	0.01	0.01	0.01	0.01
Nd	0.02	0.02	0.02	0.02	0.02	0.02
P	5.91	5.93	5.77	5.87	5.83	5.85
Si	0.00	0.00	0.00	0.00	0.00	0.00
Cl	0.34	0.44	0.59	0.59	0.57	0.30
F	1.88	1.35	1.42	1.20	1.38	1.73
OH	b.d.	b.d.	b.d.	b.d.	b.d.	b.d.